Selection for longer limbs in mice increases bone stiffness and brittleness, but does not alter bending strength

Miranda N. Cosman[1], Hayley M. Britz[2,3], Campbell Rolian[3,4]*

Author Affiliations:

[1]Department of Anthropology, University of Michigan, 101 West Hall 1085 S. University Ave, Ann Arbor, Michigan, 48109, United States

[2]Department of Cell Biology and Anatomy, Cumming School or Medicine, University of Calgary, 3330 Hospital Drive NW, Calgary, Alberta, T2N4N1, Canada.

[3]McCaig Institute for Bone and Joint Health, University of Calgary, 3330 Hospital Drive NW, Calgary, Alberta, T2N4N1, Canada

[4]Department of Comparative Biology and Experimental Medicine, Faculty of Veterinary Medicine, University of Calgary, 3330 Hospital Drive NW, Calgary, Alberta, T2N4N1, Canada.

*to whom correspondence should be addressed: cprolian@ucalgary.ca

ABSTRACT

The ability of a bone to withstand loads depends on its structural and material properties. These tend to differ among species with different modes of locomotion, reflecting their unique loading patterns. The evolution of derived limb morphologies, such as the long limbs associated with jumping, may compromise overall bone strength. We evaluated bone mechanical properties in the Longshanks mouse, which was selectively bred for increased tibia length relative to body mass. We combined analyses of 3D shape and cross-sectional geometry of the tibia, with mechanical testing, and bone composition assays, to compare bone strength, elastic properties, and mineral composition in Longshanks and in random-bred controls. Our data show that, despite being more slender, cortical geometry and predicted bending strength of the Longshanks tibia were similar to controls. In whole bone bending tests, measures of bone bending strength were similar across groups, however, Longshanks tibiae were significantly more rigid, more brittle, and required less than half the energy to fracture. Tissue-level elastic properties were altered in the same way in Longshanks, but the bones did not differ in water content, ash content, or density. These results indicate that while Longshanks bones are as strong as random-bred control tibiae, selection for increased tibia length has altered its elastic properties, possibly through changes in organic bony matrix composition. We conclude that selection for certain limb morphologies, and/or selection for rapid skeletal growth, can lead to tissue-level changes that can increase the risk of skeletal fracture, which in turn may favor the correlated evolution of compensatory mechanisms to mitigate increased fracture risk, such as delayed skeletal maturity.

INTRODUCTION

Bone fractures are an important disease burden in humans and domesticated animals (Gregory and Wilkins 1989; Fleming et al. 1994; Bouxsein 2005; Ramzan and Palmer 2011), and the ability to withstand bone fractures throughout life likely also impacts the evolutionary fitness of wild animals (Bramblett 1967; Taylor 1971; Lovell 1991; Jurmain 1997; ter Hofstede et al. 2003; Forsman et al. 2006; Carter et al. 2008). The ability of a bone to withstand external loading depends on its material properties, size, and shape, especially its cross-sectional geometry (Rubin 1984; Jepsen et al. 2003; O'Neill and Ruff 2004; Felsenberg and Boonen 2005; Hernandez and Keaveny 2006). Long bone cross-sectional geometries often differ between species that use different locomotor repertoires. This variation in bone structure may reflect differences in where and how loads are distributed across a bone (Bou et al. 1987; Bou et al. 1991; Cubo and Casinos 1998; Christiansen 1999b, a; Young et al. 2014), though this relationship does not always hold (Biewener and Bertram 1994; Demes et al. 1998; Demes et al. 2001; Lieberman et al. 2004; Wallace et al. 2014). Cross-sectional geometry and other bone properties (e.g., trabecular orientation) can also change over a lifetime in response to specific loading patterns (Biewener and Bertram 1994; Heinrich et al. 1999; Lieberman et al. 2003; Ruff 2003; Pontzer et al. 2006; Main and Biewener 2007; Young et al. 2010; Ruff et al. 2013; Sarringhaus et al. 2016). At the same time, however, the adaptive evolution of limb bone morphologies in specific locomotor contexts may also be constrained by other organismal traits such as body mass or skeletal size, leading to potential trade-offs in the strength of individual limb bones.

The Longshanks mouse was selectively bred for longer tibiae relative to body mass. In 20 generations, we produced two independent lines of Longshanks mice (hereafter LS1 and LS2) in which the tibia is ~13-15% longer than random-bred control mice from the same genetic background (CD-1, hereafter C mice), but body masses remain unchanged (Marchini et al. 2014). In our previous study using only LS1, we demonstrated that tibia length increased without a commensurate change in its cross-sectional geometry (i.e., with negative allometry) (Cosman et al. 2016). Specifically, the tibia's cross-sectional area and polar section modulus in LS1 did not change appreciably, which led us to predict that it is significantly less resistant to bending moments. In a related study (Farooq et al. 2017), we found that tibia trabecular microarchitecture had been substantially altered in parallel with increases in tibia length in both Longshanks lines, potentially altering its ability to withstand compressive loads. In the present study, we investigated whether the altered shape of the Longshanks tibia has impacted its strength and elastic properties. We performed three complementary analyses. First, we evaluated 3D

shape of the tibia as well as its cross-sectional properties at the midshaft in the three lines. This analysis extends our previous study (Cosman et al. 2016) by including both Longshanks replicates, and by examining whether shape changes remained present in Longshanks at F15, i.e., after an additional five generations of selective breeding. We tested the hypothesis that bone shape and cross-sectional properties (e.g., cross-sectional area) did not differ significantly among the three lines (Cosman et al. 2016). Second, we assessed the mechanical strength and elastic properties of the bones using a three-point bending test to test the hypothesis that there are no differences in these traits among the three lines. Finally, we compared tissue-level bone composition among the lines in terms of water and mineral content.

MATERIALS and METHODS

Samples: All animal procedures were approved by the Health Sciences Animal Care Committee at the University of Calgary (protocol AC13-0077). Mice from the F15 and F16 generations of the Longshanks experiment were used in this study. Details of the selection experiment are provided elsewhere (Marchini et al. 2014). All Longshanks and Control mice are derived from CD-1 outbred stock. At both generations, Longshanks tibiae were ~12-14% longer than in Controls, but there were no differences in mean body mass among lines. For assessing whole bone and tissue-level mechanical properties, we collected sex-balanced samples of mice that were not selected as breeders for the following generation (sample sizes: LS1: 42, LS2: 38, C: 36). To examine bone tissue composition, we sampled non-breeder females from generation F16 (n = 8 per line).

Micro-Computed Tomography (uCT) scans: Following euthanasia at 56-63 days (by CO_2 inhalation), mice were weighed to the nearest 0.01g and packed into Styrofoam tubes, and whole body uCT scans were acquired on a Skyscan 1173 uCT scanner (Bruker, Kontich, Belgium) at an isotropic resolution of 45µm (70kV voltage and 114µA current). 3D image stacks were reconstructed in NREcon v1.6.9 (Bruker, Kontich, Belgium) for shape and cross-sectional analyses.

3D Shape Analysis: Image stacks were imported into Amira v.5.4.2 (Visage Imaging, Berlin, Germany) and an Amira mesh file (.am) of the hind limb was created for shape analysis. A set of 12 3D landmarks were placed on homologous anatomical structures at the proximal and distal epiphyses, as well as the tibia-fibula junction, in the scans of the right tibia from each mouse. The protocol for shape, including reliability and measurement error of landmark placements, and geometric morphometric

analysis, are described in Cosman et al. (2016). The distance between the landmarks at the cranial point of the proximal epiphysis and on the caudal medial tip of the medial malleolus was used as a measure of tibia length.

Cross Sectional Area and Properties: The Amira mesh file was imported ImageJ 1.51p (National Institutes of Health, Bethesda, Maryland) (Rasband 2014). To account for different whole body scan positions, the stacks were first aligned vertically (parallel to long axis of tibia), using the Interactive Stack Rotation plugin in ImageJ. Following an automatic thresholding procedure, we used the BoneJ plugin (Doube et al. 2010) to obtain cross-sectional properties from a slice at the distal tip of the tibial tuberosity, i.e., the same approximate area that underwent mechanical testing. Following the recommendations put forth in Jepsen et al. (2015), we obtained periosteal area (total area, Tt.Ar. in mm^2), cortical area (Ct.Ar., in mm^2), bone marrow area (i.e., endosteal area, Ma.Ar, in mm^2), relative cortical area (Ct.Ar/Tr.Ar), mean cortical thickness (Ct.Th), the minimum and maximum moments of inertia (I_{min} and I_{max}, respectively, in mm^4) and the polar section modulus (Z_P, in mm3) at the selected slice. As in our previous study (Cosman et al., 2016), we calculated an index of robusticity (IR) by taking the ratio of Zp (in mm^3) to the product of bone length (in mm) and body mass (in $mg^{2/3}$) (Polk et al. 2000; Ruff 2000; Young et al. 2014) to evaluate the tibia's bending strength in relation to its length and the mass of the animal.

Whole Bone Mechanical Properties: A sex-balanced subsample of 82 mice were used for mechanical testing (sample sizes by sex: LS1=15F/13M, LS2=15F/15M, C=12F/14M). Mechanical testing was performed on the same day an individual mouse was scanned. After scanning, the left hind limb was skinned and removed, and dissected free of soft tissue. The bones were then subjected to a three-point bend test on an ElectroForce 3230 testing machine (Bose Corp., Eden Prairie, USA). The end fixtures (supporting points) were placed six mm apart in the Longshanks Line 1 and Line 2 and four mm apart in the Control line. This difference of 2mm, which is approximately equal to the mean length difference between Longshanks and control tibiae (see Results), ensured that bones were loaded at anatomically homologous locations in the three lines.

The center support (crosshead) was placed on the lateral side at the level of the distal end of the tibial tuberosity, corresponding to where cross-sectional properties were measured. The left support was on the tibial metaphysis and the right was placed immediately proximal to the tibia-fibula junction. The bottom fixtures were attached to a 450 N load cell, and the crosshead moved at a constant displacement rate of 2 mm/min. The tibiae were bent medio-laterally in the transverse plane as this

orientation improved stability of the bone on the test fixtures. To minimize bone movement prior to the bending test, a preload of 1N was applied, which did not cause any visible deformation of the bone. The bones were then loaded until failure.

Whole Bone Bending Tests: (1) Moment-normalized displacement curves: All mechanical testing analyses were conducted using custom-written scripts in Matlab (R2017b, Natick, MA). Three-point bending tests generate load-displacement curves that record how much force a structure can withstand before fracturing, under continuous displacement of the tester's crosshead. Because our fixture span lengths were not the same size in Longshanks and Controls, however, their load-displacement curves are not directly comparable. Normalizing both load and displacement for fixture geometry is required for two reasons. First, mechanical testers measure loads experienced by the bone, however whole-bone strength is ultimately determined by bending moments, which are a function of the distance between the tester's supports (i.e., load arms) (Jepsen et al. 2015). Second, for a given displacement of the crosshead, a bone bent on a shorter span deflects substantially more than a bone bent on a longer span. Accordingly, identical recorded displacements to fracture in these two bones would lead one to conclude erroneously that the bones are equally ductile, when in fact the bone on the shorter span undergoes more deformation before failing. Hence, we converted the bending data to moment-normalized displacement curves following (Jepsen et al. 2015). Moments of force were obtained using the following equation:

$$\text{Eq. 1: } M = FL/4$$

Where M is the moment of force, in Nmm, F is the force, and L is the span length between the two bottom points of the testing apparatus (6mm for Longshanks, 4 mm for Controls). The displacement d was normalized as follows, and is expressed in units of mm/mm^2:

$$\text{Eq. 2: } d' = 12d/(L^2)$$

Moment-normalized displacement curves (M-d') were used to obtain yield moment, at which deformation becomes plastic (see below), as well as the maximum moment and moment at fracture.

(2) Rigidity, post-yield displacement, and work-to-fracture: rigidity of the tibia, in N/mm^2, describes the amount of elastic deformation the bone undergoes as a function of the moments applied. Rigidity is derived from moment-normalized displacement, and is the fixture-normalized equivalent of whole bone stiffness derived from load-displacement plots (Jepsen et al. 2015). Rigidity was obtained as the slope of a linear regression fitted to the initial linear portion of the M-d' curves. The linear regression was fit to

the points between 15 and 25% of fracture displacement, as some individuals' M-d' curves departed from linearity after ~30% displacement. Yield was defined as the point at which a regression line representing a 10% loss in rigidity intersects the M-d' curve. Normalized post-yield displacement (PYD), in mm/mm2, was defined as the normalized displacement between yield and fracture. Finally, work-to-fracture, in N, which reflects the overall bending resistance of a structure, was obtained by integrating the area under the total M-d' curves (Jepsen et al. 2015).

Bone Tissue Mechanical Properties

Mechanical properties of bone tissue can be estimated from bending tests, using expectations derived from engineering beam theory (Turner and Burr 1993, Jepsen et al. 2015). These estimates must be interpreted with caution, however, because bones are not perfect cylinders of equal thickness throughout the cortex, and their bending behavior can depart significantly from beam theory predictions (van Lenthe et al. 2008). Still, tissue-level estimates obtained from three-point bending tests can provide a "first-pass" approximation of differences among groups when homologous bones are compared under similar testing conditions. We used the force-displacement relationships to obtain stress (σ), strain (ε), and the elastic modulus (E) using the following equations:

$$\text{Eq. 3: } \sigma = FLc/4\ I$$

$$\text{Eq. 4: } \varepsilon = 12cd/(L^2)$$

$$\text{Eq. 5 : } E = KL^3/48I$$

Where σ is stress, in N/mm^2 (MPa), ε is strain (unitless), E is elastic modulus (MPa), L is span length (mm), d is raw displacement of the testing apparatus (mm), c (mm) is the distance from the bone cross-section's centroid to the outermost point on the cortex, I is the moment of inertia of the cross-section around the bending axis, and K is stiffness (N/mm), i.e., the slope of the linear portion of the raw force-displacement plots, derived using the same method as above for rigidity. Because tibiae were bent in a mediolateral plane, we took c to be half the minimum caliper diameter and I to be I_{max}, both obtained from BoneJ's cross-sectional geometry output (see above). We used the stress-strain curves to derive yield strength and ultimate strength using the same method as above for yield and maximum moments.

Bone Tissue Composition

The left tibiae of previously frozen F16 female mice were dissected and cleared of soft tissue (n = 8 per line, each comprising four pairs of siblings from separate families). Bones were trimmed to obtain sections of tibia diaphysis, by sectioning the bones with a razor blade distal to the proximal metaphysis, and immediately proximal to the tibia-fibula junction. The tibia sections were flushed with water to expel marrow. To obtain hydrated tissue weights, the bones were centrifuged at 5,000 g for 5 minutes, and weighed to the nearest 0.1 mg on an analytical balance. Dry tissue weight was determined after drying the bone sections overnight at 60°C. Next, the bone segments were scanned on a Skyscan 1173 uCT scanner (Bruker, Kontich, Belgium) at an isotropic resolution of 10µm (70kV voltage and 114µA current). 3D image stacks were reconstructed in NREcon v1.6.9 (Bruker, Kontich, Belgium), and the "Volume Fraction" module in BoneJ was used to obtain dry bone volume. Finally, ash weight was obtained after ashing the bones in a muffle furnace at 600°C for 24 hours. Dry bone density was obtained as dry bone weight (mg) divided by dry bone volume (mm^3). Water and ash content measures were expressed as a percentage of hydrated weight assuming a water density of 1 (Jepsen et al. 2001).

Statistical Analysis:

Tibia Shape: Geometric morphometric analyses were carried out in MorphoJ v.104a (Klingenberg 2011). The 12-variable 3D landmark dataset was first subjected to a general least squares Procrustes superimposition (Dryden and Mardia 1998; Slice 2005). Shape differences between the groups were explored by means of principal components analysis (PCA) on Procrustes shape variables. Statistical significance of any difference in mean shape was assessed by pairwise discriminant function analyses (DFA), followed by permutation tests (1000x), as implemented in MorphoJ. Changes along principal components were visualized by means of deformations of wireframes that described shape in the medio-lateral, antero-posterior and proximo-distal epiphyseal profiles of the tibia.

Cross-Sectional, Whole Bone and Tissue Properties: All statistical analyses were performed in Matlab using custom scripts (R2017b, Natick, MA). Cross-sectional and strength properties were compared among the three groups using analyses of covariance (ANCOVA), with mouse line and sex as categorical factors, and body mass as a covariate representing an animal's overall size. Our preliminary analyses showed that, aside from bending moments (see Results), there was no interaction between sex and line for bone geometric and strength properties, thus all subsequent statistical analyses were carried out on

samples with sexes pooled within lines. We used Tukey's post-hoc tests to test for statistical significance of pairwise differences in the marginal means among the lines. Differences among females in the F16 lines in tissue density and composition were determined using ANOVAs, followed by Tukey's post-hoc tests. In all tests, an alpha value of less than 0.05 was considered statistically significant.

RESULTS

Morphometrics and 3D Shape:

The sample of LS1 mice used in this study was significantly heavier than the other lines (Table 1), even though mean body mass among the complete F15 populations is the same (data not shown). This discrepancy is most likely a stochastic artifact of subsampling from the lines. Among lines (pooled by sex), mean tibia length was ~13% greater in Longshanks, but did not differ between LS1 and LS2. In terms of 3D shape both Longshanks lines were significantly different from Control in mean shape (DFA, mean Procrustes distances: 0.024 [LS1 vs C], 0.019 [LS2 vs C], both permutation test T-square statistics $p<0.001$). As in our previous analysis conducted on F10 tibiae (Cosman et al. 2016), F15 LS1 tibiae are more gracile, with relatively smaller cross-sectional area of the proximal epiphysis, and narrower proximal shafts in the craniocaudal direction (Figure 1). Our analysis also showed a similar gracilization in LS2 tibiae. Interestingly, however, discriminant function analyses also showed that LS1 and LS2 differed in mean shape (mean Procrustes distance: 0.012, T-square statistic: 171.5, $p=0.003$), with LS1 having slightly more gracile cross-sections (Figure 1).

Cross Sectional Geometry:

Cross-sectional properties of the tibia mid-shaft in all three lines (sexes pooled) are broadly similar. One notable difference is the endosteal area (Ma.Ar.), which is significantly greater in the Longshanks lines than in Control (Table 1). Coupled with marginally larger periosteal areas, these larger endosteal areas contribute to significantly lower relative cortical areas in Longshanks (Ct.Ar./Tt.Ar.). The minimum and maximum moments of inertia are not significantly different among lines, nor is the mean index of robusticity, predicting the whole bone bending strength based on geometric properties, length of the tibia and body mass should be similar among lines.

Whole Bone Material Properties in Bending:

In the bending tests, the tibiae of several individuals did not fracture before the bottom and top supports came into contact. In this situation, displacement becomes limited but the moments continue to be experienced by the bone at a constant rate, leading to incorrect estimates for the post-yield displacements and work-to-fracture. Consequently, we removed these individuals from all strength analyses (n=17). Within line, twice as many Control individuals were removed from the analysis (LS1: 4 out of n = 27, LS2: 4/29, C: 9/26, 3-group chi-square test, $X^2 = 4.47$, p=0.107).

We found a statistically significant interaction between line and sex for moment variables, however this interaction was driven primarily by LS1, in which moments were significantly greater in males than in females from all lines. When pooled by sex, there were no significant differences among lines in mean yield, maximum, or fracture moments (Table 2, Figure 2A). In contrast, the normalized yield and post-yield displacements are significantly shorter in both Longshanks lines, leading to a total displacement that is less than half as great as for Controls. The shorter normalized PYD indicates a significantly more brittle bone in Longshanks. Similarly, Longshanks' tibia is significantly more rigid (Table 2, Figure 2A). Taken together, the similar bending moments but different mean normalized deflections in Controls vs Longshanks tibiae contribute to a mean normalized work-to-fracture in both Longshanks lines that is approximately half its value in Control.

Bone Tissue Mechanical Properties

The bone tissue strength properties estimated by combining three-point bending and cross-sectional geometry data are consistent with the whole bone bending data (Figure 2B, Table 2). Specifically, we found no differences among lines in the yield and ultimate strengths of bone tissue, however the mean estimated elastic modulus, which reflects the resistance to deformation when bone tissue is loaded, is approximately twice as great in Longshanks as it is in Control tibiae.

Bone Tissue Composition

There was no difference in mean mass among the F16 females used for bone composition (Table 3). Mean water content was ~8% higher in Longshanks bones, while ash content and dry bone density differed by less than 2%. We found no statistically significant differences among the lines in water content, dry density, or in the proportion of mineralized tissue (Figure 3, Table 3).

DISCUSSION

In this study, we tested whether whole bone and tissue-level mechanical properties, as well as bone composition, were altered by changes in length and shape of the tibia in a mouse selectively bred for greater tibia length relative to body mass. Our shape analysis confirms and extends our previous observations in Longshanks line LS1 at generation F10, in that the tibia in both Longshanks lines has become more gracile at generation F15, when compared to the random-bred Control mice (Cosman et al. 2016). Furthermore, the cross-sectional geometry at the midshaft in all three lines was similar, with the exception of the lower relative cortical area in Longshanks, which is likely due to their slightly larger endosteal cavities. Our whole bone mechanical testing on the tibia revealed significant differences in the bending behavior of Longshanks vs Control bones. In accordance with the broadly similar midshaft cross-sectional properties among lines, we found no differences among lines in the yield, maximum, and fracture moments experienced by the tibia in whole bone bending (Figure 2A). In other words, despite being longer by ~13% relative to body mass, the Longshanks tibiae remain appropriately buttressed against external bending moments. This pattern holds when looking at tissue-level yield and ultimate strengths, which did not differ significantly among lines (Figure 2B).

In contrast, Longshanks and Control bones exhibited striking differences in the elastic properties of the bones. Specifically, in whole bone bending, Longshanks tibiae were significantly more rigid, experiencing bending moments that were over twice as great per unit of normalized displacement relative to Controls (Figure 2A, Table 2). Furthermore, normalized displacements to yield and post-yield displacement to fracture were half as great as in Controls, indicating bones that were also more brittle in addition to their increased rigidity. Due in part to this increased rigidity and brittleness, the average work required to break a Longshanks tibia was 45-55% lower than that required to break a Control tibia. These changes in the elastic properties of the bones were further supported by our observation that a third of Control tibiae were removed from the strength analysis because their bending displacements exceeded the mechanical tester's maximum travel distance, while only ~14-15% of the Longshanks bones had to be excluded for this reason (3-group chi-square test, $X^2 = 4.47$, $p=0.107$).

At the tissue level, our estimates of elastic modulus, a measure of the resistance of a unit of bone tissue to deformation when loaded, suggest that the observed increase in rigidity of the Longshanks tibia may arise from changes in the mechanical properties of cortical bone tissue itself, more so than from changes in its cortical geometry or overall shape. Whole bone strength is influenced by both structural *and* material properties of bones, however brittleness is thought to reflect the tissue-level material properties of bone, such as bone mineralization and/or bone matrix composition (Jepsen et al. 1996; Jepsen et al. 2001; Wang et al. 2001; Silva et al. 2006). In this context, the greater elastic modulus and brittleness of Longshanks suggest that its cortical tissue properties may have been altered as a correlated response to selection for increased relative limb bone length.

To examine this possibility, we quantified basic bone composition on samples of F16 tibia diaphyses in the three groups. Bone composition data showed that neither water content, nor mineral content, nor dry bone density differed among the lines (Figure 3). These data are in agreement with our previous analyses of the tibia metaphysis and shaft in Longshanks. Using complementary micro-CT based methods, Farooq et al. (2017) found that tissue mineral density (TMD) was *lower* by ~ 7% in LS1 compared with Controls and LS2, while the TMD of LS2 is the same as Controls. This trend can be observed in the present ash content analysis, although the difference is much smaller, and not statistically significant (~1.5% lower in LS1 compared with C, Table 3, Figure 3). We may tentatively exclude mineral content as the basis of Longshanks' brittle bones, however, because increased mineralization is associated with *increased* stiffness/brittleness of bone tissue (Currey 1999; Jepsen et al. 2001; Mulder et al. 2008). Moreover, Farooq et al. (2017) found no differences in cortical microarchitecture based on high resolution x-ray microscopy of the tibia diaphysis, including porosity.. Absent changes in tissue mineral composition and microarchitecture, this suggests that the molecular organization and composition of the organic bony matrix itself may be altered in Longshanks in ways that contribute to its brittleness. Future work that directly assesses elastic modulus, cortical matrix composition, including collagen fibril content, orientation and organization (Martin and Ishida 1989), will help to determine whether selection for longer tibiae altered the molecular and/or developmental properties of Longshanks' brittle bones.

Broader Implications: We have shown that selection for increased relative tibia length, mediated largely by accelerated longitudinal growth (Marchini and Rolian 2018), did not alter whole bone bending strength, but substantially increased rigidity and brittleness of the tibia, in as few as 15 generations of

selective breeding (~3.5 years). Although caution is warranted in generalizing from this experimental system, our results have implications for bone mechanical properties in the evolution of functional specializations in other species, both domestic and wild. For example, our data indicate that selection for accelerated skeletal growth can increase bone brittleness. In an analysis comparing domestic White Leghorn chickens selectively bred for rapid growth in body mass to their putative ancestral stock, the Red Junglefowl, Rubin et al. (2007) showed that the former have longer femora, and substantially increased stiffness and reduced PYD, similar to Longshanks. This increased brittleness occurred even though the White Leghorn's body mass, bone mineral contents, and cortical geometries also responded to selection in ways that improve bone strength (Rubin et al. 2007; Wright et al. 2010). Similarly, the greyhound, a sprinting dog breed selectively bred for long, tapered limbs, has significantly stiffer and more brittle bones than the pit bull, a breed selectively bred for fighting (Kemp et al. 2004, 2005).

In wild species, evolution of long, tapered limbs related to functional specializations such as sprinting or leaping, could similarly lead to changes in the elastic properties of the long bones, e.g., increasing their stiffness while reducing their ductility. Should these long bones experience bending moments that cause deformations beyond the elastic region (i.e., past its yield point), then increased brittleness may make them more prone to fracture. While it is not known how often this happens in the wild, an increased fracture risk presumably carries negative fitness consequences (Bramblett 1967; Taylor 1971; Bulstrode et al. 1986; Bertram and Biewener 1988; Lovell 1991; Jurmain 1997; ter Hofstede et al. 2003; Forsman et al. 2006; Carter et al. 2008), and thus over evolutionary timescales this may favor the correlated evolution of compensatory mechanisms that help to mitigate the impact of long tapered bones on fracture risk. Such mechanisms could include structural changes of the limb long bones, such as fusion of bony elements (Moore et al. 2015) and/or changes in life history traits including delayed skeletal maturation to maintain growth rates within physiologically optimal ranges for bony matrix synthesis. For example, a study of 25 families of non-passerine birds found a positive correlation between wing length and fledgling periods (Carrier and Auriemma 1992). Powered flight may be ontogenetically delayed in these species in order to maintain limb bone growth rates within a safe range for their structural integrity. Further analyses, especially in mammals, will be necessary to test the complex relationships between life history and skeletal physiology and strength.

Author Contributions: Study Design: MNC, CR; Data Collection: MNC, HMB; Data Analysis: MNC, CR, Manuscript Preparation: MNC, HMB, CR.

Acknowledgements

We thank Jason Anderson and Jessica Theodor for providing access to the SkyScan uCT scanner, Nigel Shrive and Neil Duncan for access to the Bose mechanical tester, and Anne Katzenberg and Kris Markin for facilitating access to the muffle furnace. Many thanks also to Karl Jepsen, John Bertram and Sarah Manske, as well as to the editor and two anonymous reviewers for helpful feedback on previous versions of the manuscript.

Funding

This study was supported by Discovery Grant 4181932 from the Natural Sciences and Engineering Research Council of Canada (NSERC) to CR, by the University of Calgary Faculty of Veterinary Medicine, by an award from the Program for Undergraduate Research Experience (PURE) to MNC, and by an NSERC Alexander Graham Bell Canadian Graduate Scholarship and Alberta Innovates Health Services Incentives Scholarship to HMB.

Competing Interests

The authors declare no competing interests.

Data availability

All shape, cross-sectional, strength and ash data can be found in Supplementary File S1.

References

Bertram, J. E. A. and A. A. Biewener. 1988. Bone Curvature - Sacrificing Strength for Load Predictability. J Theor Biol 131:75-92.

Biewener, A. A. and J. E. Bertram. 1994. Structural response of growing bone to exercise and disuse. J Appl Physiol 76:946-955.

Bou, J., A. Casinos, and J. Ocana. 1987. Allometry of the Limb Long Bones of Insectivores and Rodents. J Morphol 192:113-123.

Bou, J., M. Olmos, and A. Casinos. 1991. Strengths of the Limb Bones of Birds and Small Mammals in Bending and Twisting. Annales Des Sciences Naturelles-Zoologie Et Biologie Animale 12:197-207.

Bouxsein, M. L. 2005. Determinants of skeletal fragility. Best Practice & Research Clinical Rheumatology 19:897-911.

Bramblett, C. A. 1967. Pathology in Darajani Baboon. Am J Phys Anthropol 26:331-+.

Bulstrode, C., J. King, and B. Roper. 1986. What Happens to Wild Animals with Broken Bones. Lancet 1:29-31.

Carrier, D. R. and J. Auriemma. 1992. A developmental constraint on the fledging time of birds. Biol J Linn Soc 47:61-77.

Carter, M. L., H. Pontzer, R. W. Wrangham, and J. K. Peterhans. 2008. Skeletal pathology in Pan troglodytes schweinfurthii in Kibale National Park, Uganda. Am J Phys Anthropol 135:389-403.

Christiansen, P. 1999a. Scaling of mammalian long bones: small and large mammals compared. J Zool 247:333-348.

Christiansen, P. 1999b. Scaling of the limb long bones to body mass in terrestrial mammals. J Morphol 239:167-190.

Cosman, M. N., L. M. Sparrow, and C. Rolian. 2016. Changes in shape and cross-sectional geometry in the tibia of mice selectively bred for increases in relative bone length. J Anat 220:940-951.

Cubo, J. and A. Casinos. 1998. The variation of the cross-sectional shape in the long bones of birds and mammals. Annales Des Sciences Naturelles-Zoologie Et Biologie Animale 19:51-62.

Currey, J. D. 1999. What determines the bending strength of compact bone? J Exp Biol 202:2495.

Demes, B., Y. X. Qin, J. T. Stern, S. G. Larson, and C. T. Rubin. 2001. Patterns of strain in the macaque tibia during functional activity. Am J Phys Anthropol 116:257-265.

Demes, B., J. T. Stern, M. R. Hausman, S. G. Larson, K. J. McLeod, and C. T. Rubin. 1998. Patterns of strain in the macaque ulna during functional activity. Am J Phys Anthropol 106:87-100.

Doube, M., M. M. Klosowski, I. Arganda-Carreras, F. P. Cordelieres, R. P. Dougherty, J. S. Jackson, B. Schmid, J. R. Hutchinson, and S. J. Shefelbine. 2010. BoneJ Free and extensible bone image analysis in ImageJ. Bone 47:1076-1079.

Dryden, I. L. and K. V. Mardia. 1998. Statistical shape analysis. John Wiley & Sons, Chichester ; New York.

Felsenberg, D. and S. Boonen. 2005. The bone quality framework: Determinants of bone strength and their interrelationships, and implications for osteoporosis management. Clin Ther 27:1-11.

Fleming, R. H., C. C. Whitehead, D. Alvey, N. G. Gregory, and L. J. Wilkins. 1994. Bone-Structure and Breaking Strength in Laying Hens Housed in Different Husbandry Systems. Br Poult Sci 35:651-662.

Forsman, E. D., I. A. Otto, and E. Muths. 2006. Healed Fractures and Other Abnormalities in Bones of Small Mammals. Northwest Nat 87:143-146.

Gregory, N. G. and L. J. Wilkins. 1989. Broken Bones in Domestic-Fowl - Handling and Processing Damage in End-of-Lay Battery Hens. Br Poult Sci 30:555-562.

Heinrich, R. E., C. B. Ruff, and J. Z. Adamczewski. 1999. Ontogenetic changes in mineralization and bone geometry in the femur of muskoxen (Ovibos moschatus). J Zool 247:215-223.
Hernandez, C. J. and T. M. Keaveny. 2006. A biomechanical perspective on bone quality. Bone 39:1173-1181.
Jepsen, K. J., O. Akkus, R. J. Majeska, and J. H. Nadeau. 2003. Hierarchical relationship between bone traits and mechanical properties in inbred mice. Mamm Genome 14:97-104.
Jepsen, K. J., S. A. Goldstein, J. L. Kuhn, M. B. Schaffler, and J. Bonadio. 1996. Type-I collagen mutation compromises the post-yield behavior of Mov13 long bone. J Orthop Res 14:493-499.
Jepsen, K. J., D. E. Pennington, Y. L. Lee, M. Warman, and J. Nadeau. 2001. Bone brittleness varies with genetic background in A/J and C57BL/6J inbred mice. J Bone Miner Res 16:1854-1862.
Jepsen, K. J., M. J. Silva, D. Vashishth, X. E. Guo, and M. C. H. van der Meulen. 2015. Establishing Biomechanical Mechanisms in Mouse Models: Practical Guidelines for Systematically Evaluating Phenotypic Changes in the Diaphyses of Long Bones. J Bone Miner Res 30:951-966.
Jurmain, R. 1997. Skeletal evidence of trauma in African apes, with special reference to the Gombe chimpanzees. Primates 38:1-14.
Kemp, T. J., K. N. Bachus, J. A. Nairn, and D. R. Carrier. 2004. Mechanical properties of limb bones in dogs specialized for running versus fighting. Integr Comp Biol 44:712-712.
Kemp, T. J., K. N. Bachus, J. A. Nairn, and D. R. Carrier. 2005. Functional trade-offs in the limb bones of dogs selected for running versus fighting. J Exp Biol 208:3475-3482.
Klingenberg, C. P. 2011. MorphoJ: an integrated software package for geometric morphometrics. Mol Ecol Resour 11:353-357.
Lieberman, D. E., O. M. Pearson, J. D. Polk, B. Demes, and A. W. Crompton. 2003. Optimization of bone growth and remodeling in response to loading in tapered mammalian limbs. J Exp Biol 206:3125-3138.
Lieberman, D. E., J. D. Polk, and B. Demes. 2004. Predicting long bone loading from cross-sectional geometry. Am J Phys Anthropol 123:156-171.
Lovell, N. C. 1991. An Evolutionary Framework for Assessing Illness and Injury in Nonhuman-Primates. Yearbook of Physical Anthropology 34:117-155.
Main, R. P. and A. A. Biewener. 2007. Skeletal strain patterns and growth in the emu hindlimb during ontogeny. J Exp Biol 210:2676-2690.
Marchini, M. and C. Rolian. 2018. Artificial selection sheds light on developmental mechanisms of limb elongation. Evolution 72:825-837.
Marchini, M., L. M. Sparrow, M. N. Cosman, A. S. Dowhanik, C. B. Krueger, B. Hallgrimsson, and C. Rolian. 2014. Impacts of genetic correlation on the independent evolution of body mass and skeletal size in mammals. BMC Evol Biol 14:258.
Martin, R. B. and J. Ishida. 1989. The Relative Effects of Collagen Fiber Orientation, Porosity, Density, and Mineralization on Bone Strength. J Biomech 22:419-&.
Moore, Talia Y., Chris L. Organ, Scott V. Edwards, Andrew A. Biewener, Clifford J. Tabin, Farish A. Jenkins Jr, and Kimberly L. Cooper. 2015. Multiple Phylogenetically Distinct Events Shaped the Evolution of Limb Skeletal Morphologies Associated with Bipedalism in the Jerboas. Curr Biol 25:2785-2794.
Mulder, L., J. H. Koolstra, J. M. J. den Toonder, and T. M. G. J. van Eijden. 2008. Relationship between tissue stiffness and degree of mineralization of developing trabecular bone. Journal of Biomedical Materials Research Part A 84A:508-515.
O'Neill, M. C. and C. B. Ruff. 2004. Estimating human long bone cross-sectional geometric properties: a comparison of noninvasive methods. J Hum Evol 47:221-235.

Polk, J. D., B. Demes, W. L. Jungers, A. R. Biknevicius, R. E. Heinrich, and J. A. Runestad. 2000. A comparison of primate, carnivoran and rodent limb bone cross-sectional properties: are primates really unique? J Hum Evol 39:297-325.
Pontzer, H., D. E. Lieberman, E. Momin, M. J. Devlin, J. D. Polk, B. Hallgrimsson, and D. M. L. Cooper. 2006. Trabecular bone in the bird knee responds with high sensitivity to changes in load orientation. J Exp Biol 209:57-65.
Ramzan, P. H. L. and L. Palmer. 2011. Musculoskeletal injuries in Thoroughbred racehorses: A study of three large training yards in Newmarket, UK (2005-2007). Vet J 187:325-329.
Rasband, W. 2014. ImageJ. U. S. National Institutes of Health, Bethesda, MD.
Rubin, C. J., H. Brandstrom, D. Wright, S. Kerje, U. Gunnarsson, K. Schutz, R. Fredriksson, P. Jensen, L. Andersson, C. Ohlsson, H. Mallmin, S. Larsson, and A. Kindmark. 2007. Quantitative trait loci for BMD and bone strength in an intercross between domestic and wildtype chickens. J Bone Miner Res 22:375-384.
Rubin, C. T. 1984. Skeletal Strain and the Functional-Significance of Bone Architecture. Calcif Tissue Int 36:S11-S18.
Ruff, C. 2003. Ontogenetic adaptation to bipedalism: age changes in femoral to humeral length and strength proportions in humans, with a comparison to baboons. J Hum Evol 45:317-349.
Ruff, C. B. 2000. Body size, body shape, and long bone strength in modern humans. J Hum Evol 38:269-290.
Ruff, C. B., M. L. Burgess, T. G. Bromage, A. Mudakikwa, and S. C. McFarlin. 2013. Ontogenetic changes in limb bone structural proportions in mountain gorillas (Gorilla beringei berirtgei). J Hum Evol 65:693-703.
Sarringhaus, L. A., L. M. MacLatchy, and J. C. Mitani. 2016. Long bone cross-sectional properties reflect changes in locomotor behavior in developing chimpanzees. Am J Phys Anthropol 160:16-29.
Silva, M. J., M. D. Brodt, B. Wopenka, S. Thomopoulos, D. Williams, M. H. M. Wassen, M. Ko, N. Kusano, and R. A. Bank. 2006. Decreased collagen organization and content are associated with reduced strength of demineralized and intact bone in the SAMP6 mouse. J Bone Miner Res 21:78-88.
Slice, D. E. 2005. Modern morphometrics in physical anthropology. Kluwer Academic/Plenum Publishers, New York.
Taylor, M. E. 1971. Bone Diseases and Fractures in East African Viverridae. Can J Zool 49:1035-&.
ter Hofstede, H. M., J. Miller, J. M. Ratcliffe, and M. B. Fenton. 2003. A healed fractured radius in a flying big brown bat (Eptesicus fuscus). J Wildlife Rehabil 26:4-7.
van Lenthe, G. H., R. Voide, S. K. Boyd, and R. Muller. 2008. Tissue modulus calculated from beam theory is biased by bone size and geometry: Implications for the use of three-point bending tests to determine bone tissue modulus. Bone 43:717-723.
Wallace, I. J., B. Demes, C. Mongle, O. M. Pearson, J. D. Polk, and D. E. Lieberman. 2014. Exercise-Induced Bone Formation Is Poorly Linked to Local Strain Magnitude in the Sheep Tibia. PLoS One 9.
Wang, X. D., R. A. Bank, J. M. TeKoppele, and C. M. Agrawal. 2001. The role of collagen in determining bone mechanical properties. J Orthop Res 19:1021-1026.
Wright, D., C. J. Rubin, A. M. Barrio, K. Schutz, S. Kerje, H. Brandstrom, A. Kindmark, P. Jensen, and L. Andersson. 2010. The genetic architecture of domestication in the chicken: effects of pleiotropy and linkage. Mol Ecol 19:5140-5156.
Young, J. W., R. Danczak, G. A. Russo, and C. D. Fellmann. 2014. Limb bone morphology, bone strength, and cursoriality in lagomorphs. J Anat 225:403-418.
Young, J. W., D. Fernandez, and J. G. Fleagle. 2010. Ontogeny of long bone geometry in capuchin monkeys (Cebus albifrons and Cebus apella): implications for locomotor development and life history. Biol Lett 6:197-200.

Tables

Table 1: Least squares means and standard errors of the cross-sectional properties at the tibia midshaft in the three lines, estimated at the covariate mean (body mass, 36.32g). Superscripts denote significant differences in LS means ($p < 0.05$) between a given group and: ^{C}Line C, ^{LS1}Line 1, ^{LS2}Line (Tukey's HSD).

Property	**Line LS1 (n=42)**	**Line LS2 (n=37)**	**Line C (n=36)**
Body mass (g)	38.03 (0.78) ^{LS2,C}	35.65 (0.54) ^{LS1}	34.92 (0.75) ^{LS1}
Tibia Length (mm)	20.13 (0.09) ^{C}	20 (0.09) ^{C}	17.86 (0.09) ^{LS1,LS2}
Ct.Ar. (mm^2)	1.37 (0.03)	1.41 (0.03)	1.41 (0.03)
Ma.Ar. (mm^2)	0.71 (0.03) ^{LS2,C}	0.82 (0.03) ^{LS1,C}	0.61 (0.03) ^{LS1,LS2}
Tt.Ar. (mm^2)	2.08 (0.05)	2.23 (0.05) ^{C}	2.02 (0.05) ^{LS2}
Rel. cortical area (Ct.Ar/Tt.Ar.)	0.66 (0.01) ^{LS2,C}	0.63 (0.01) ^{LS1,C}	0.7 (0.01) ^{LS1,LS2}
Ct.Th. (mm)	0.35 (0.01)	0.35 (0.01)	0.37 (0.01)
Min caliper diameter (mm)	1.47 (0.02)	1.52 (0.02)	1.47 (0.02)
Max caliper diameter (mm)	2.52 (0.03)	2.52 (0.03)	2.48 (0.03)
I_{min} (mm^4)	0.21 (0.01)	0.24 (0.01)	0.21 (0.01)
I_{max} (mm^4)	0.62 (0.02)	0.66 (0.03)	0.59 (0.03)
Z_{pol} (mm^3)	0.59 (0.02)	0.64 (0.02) ^{C}	0.57 (0.02) ^{LS2}
Robusticity*	0.27 (0.01)	0.29 (0.01)	0.29 (0.01)

* The values for robusticity have been multiplied by 10^5 to improve readability

Table 2: Least squares means and standard errors of the bending strength at the tibia midshaft in the three lines, estimated at the covariate mean (body mass, 36.18g). Superscripts denote significant differences in LS means ($p < 0.05$) between a given group and: ^{C}Line C, ^{LS1}Line 1, ^{LS2}Line (Tukey's HSD).

Property	**Line LS1 (n=23)**	**Line LS2 (n=25)**	**Line C (n=17)**
Body mass	38.689 (1.121) ^{C}	35.184 (0.604)	34.565 (1.012)
Tibia Length	19.972 (0.108) ^{C}	19.96 (0.099) ^{C}	17.846 (0.122) ^{LS1,LS2}
Yield moment (Nmm)	23.064 (1.33)	25.333 (1.206)	22.377 (1.504)
Maximum moment (Nmm)	25.26 (1.46)	26.32 (1.36)	23.97 (1.68)
Fracture moment (Nmm)	22.22 (1.67)	22.89 (1.52)	22.92 (1.89)
Normalized displacement to yield (mm/mm^2)	0.087 (0.009) ^{C}	0.093 (0.007) ^{C}	0.205 (0.01) ^{LS1,LS2}
Normalized post-yield displacement (mm/mm^2)	0.103 (0.016) ^{C}	0.116 (0.015) ^{C}	0.22 (0.019) ^{LS1,LS2}
Rigidity (Nmm^2)	303.5 (18.53) ^{C}	307.19 (16.49) ^{C}	136.16 (20.95) ^{LS1,LS2}
Work to fracture (N)	3.269 (0.41) ^{C}	4.011 (0.384) ^{C}	7.368 (0.463) ^{LS1,LS2}
Yield strength (MPa)	28.42 (1.77)	31.63 (1.68)	29.25 (2.28)
Ultimate strength (MPa)	30.8 (1.79)	32.88 (1.7)	31.12 (2.31)
Elastic modulus (MPa)	498.44 (28.62) ^{C}	517.86 (27.1) ^{C}	253.63 (36.81) ^{LS1,LS2}

Table 3: Observed means and standard errors of bone composition and density.

Property	**Line LS1 (n=8)**	**Line LS2 (n=8)**	**Line C (n=8)**
Body mass (g)	32.58 (0.97)	30.57 (0.73)	29.97 (1.32)
Water Content (%)	7.98 (0.83)	7.76 (0.88)	7.27 (0.95)
Ash Content (%)	62.74 (0.69)	62.98 (0.89)	63.73 (0.47)
Bone Density (mg/mm^3)	1.76 (0.01)	1.74 (0.02)	1.74 (0.02)

Figures

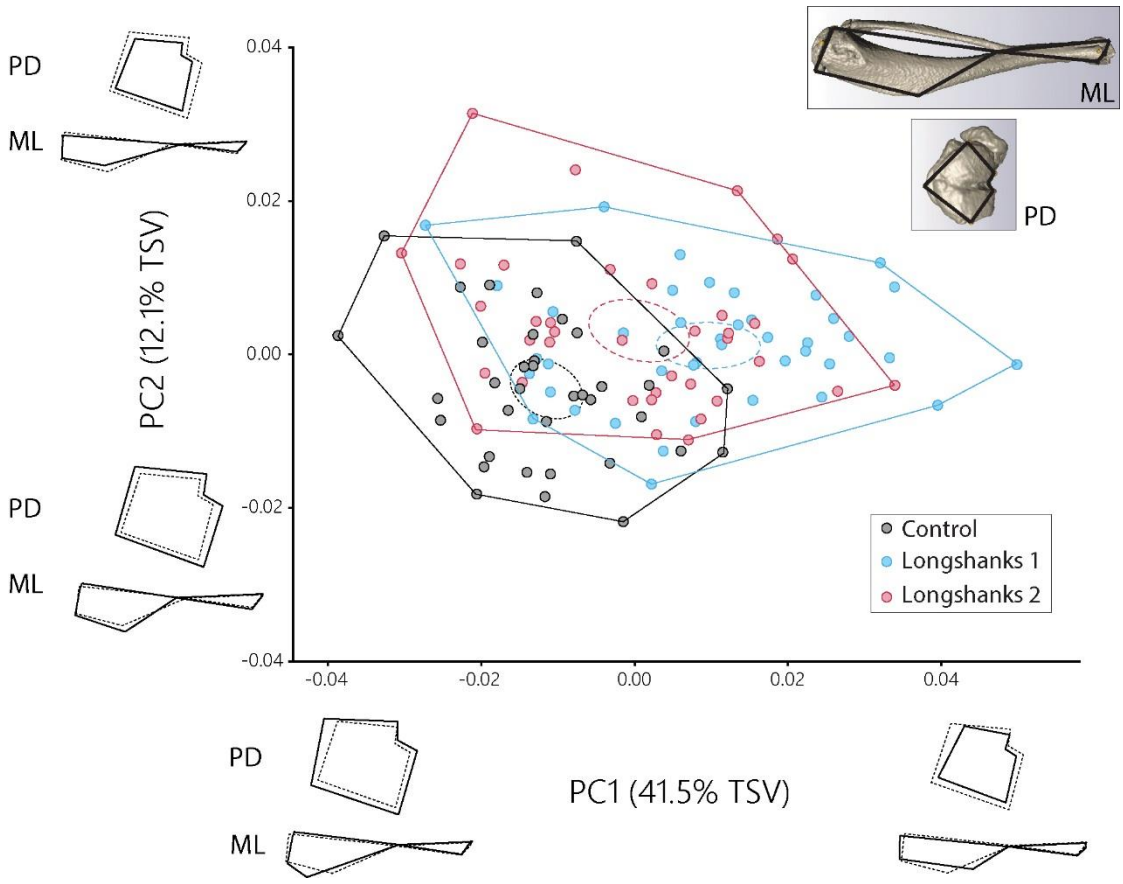

Figure 1: Scatterplots of the first two principal components (PCs) of the Procrustes shape coordinates of the tibia. Ellipses represent the 95% confidence intervals of the mean PC scores of each group (Longshanks 1 = blue, Longshanks 2 = red, and Control = black). Black wireframes along each axis illustrate the shape deformations in relation to the mean shape (dashed wireframes) associated with moving from one extreme PC score to another in the medio-lateral (ML), and proximo-distal (PD) profiles of the tibia. The inset (top right) shows the wireframes superimposed on a sample bone viewed in ML and PD profiles. TSV = total shape variance

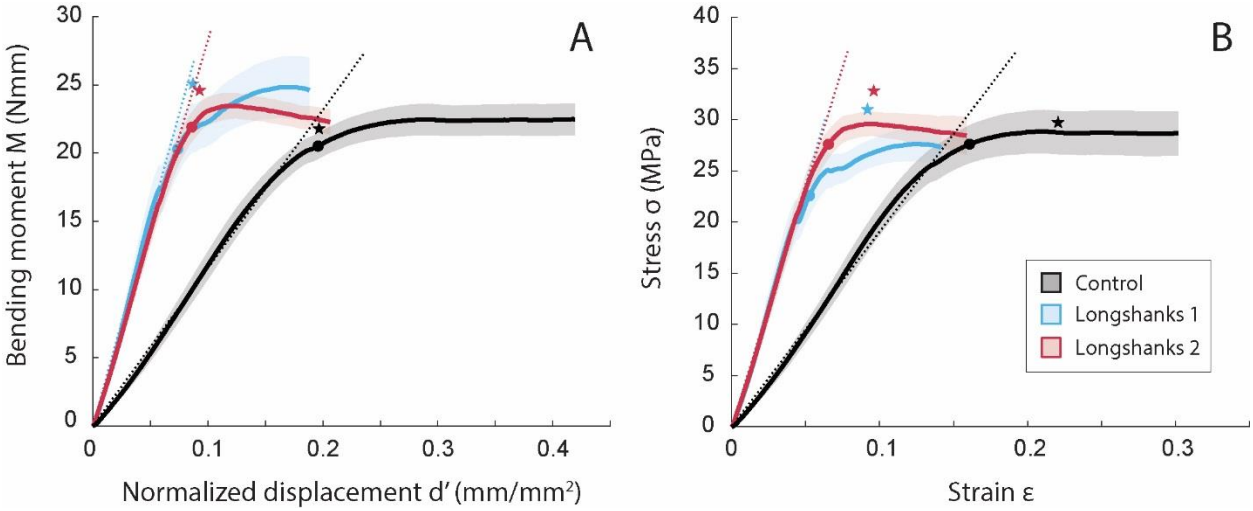

Figure 2: Mean moment-normalized displacement (A) and stress-strain curves (B) at the tibia midshaft in Longshanks 1 (blue), Longshanks 2 (red), and Control (black). Shaded area represents the mean ± SEM. Dotted lines represent the line of best fit through the linear portion of the mean moment-normalized displacement curves, prior to yield, which is indicated by a dot. The asterisks denote the normalized yield displacement/strain and yield moments/stress obtained from individual samples, averaged by line (see Table 2) The slopes of the dotted lines represent bending rigidity (A) and elastic modulus (B) (Table 2).

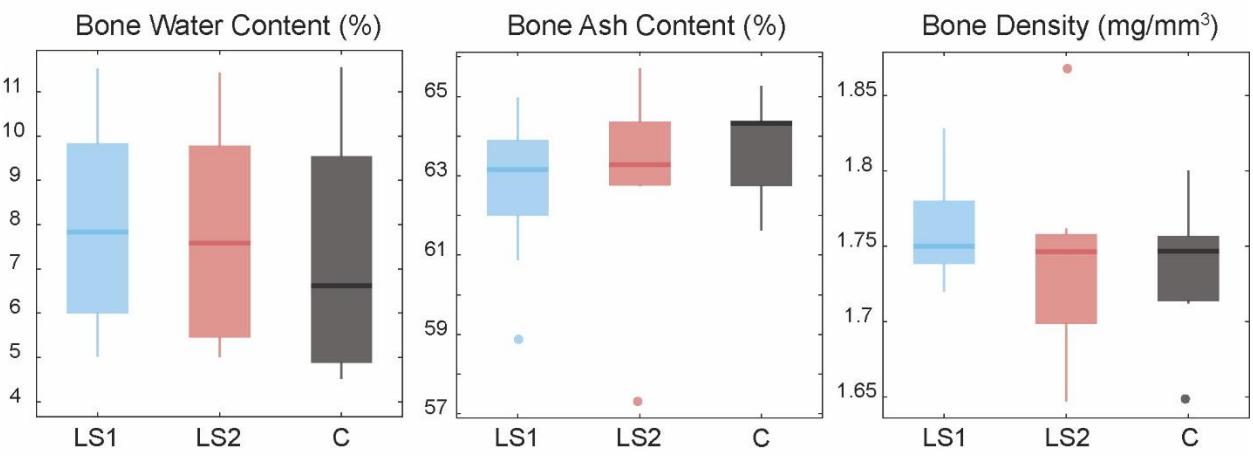

Figure 3: Tissue composition of the tibia diaphysis. Boxplots show the median (line), interquartile range (box), non-outlier range (whiskers) and outliers (circles) of each variable in Longshanks 1 (LS1, blue), Longshanks 2 (LS2, red), and Control (C, black).

Supplementary File S1.

Click here to Download File S1